

Method of calibration to correct for cloud-induced wavelength shifts in the Aura satellite's Ozone Monitoring Instrument

Robert Voors, Marcel Dobber, Ruud Dirksen, and Pieter Levelt

The in-flight wavelength calibration for the Ozone Monitoring Instrument is discussed. The observed variability in the wavelength scale is two orders of magnitude larger than caused by temperature changes in the instrument. These wavelength variations are the result of rapid changes in time in the radiance levels during an individual observation in the presence of clouds or snow and ice. We have developed a data processing method to account and correct for these changes. In February 2005 this correction was implemented in the official data processing stream. We explain in detail how and how accurately this method works. Before correction, the error in the wavelength scale can be as much as a few tenths of a pixel; after correction it is mostly less than 1/100th of a pixel, which is the required preflight accuracy. This means that higher-level products such as the total column amounts of ozone, NO₂, and SO₂ are not significantly affected. It is expected that these wavelength variations will be observed in other hyperspectral Earth observation spectrometers and that the correction mechanism should apply equally well. © 2006 Optical Society of America

OCIS codes: 300.6540, 080.2740, 300.6550, 120.4640, 280.1310, 300.6190.

1. Introduction

The ozone monitoring instrument (OMI) is one of four instruments aboard the EOS–Aura satellite and is the result of a collaboration between Dutch and Finnish institutes. Aura was launched successfully on 15 July 2004 and orbits the Earth in a Sun-synchronous orbit at an altitude of ~700 km, passing the equator northward at 13:42 local time. The Aura mission is to observe the Earth's atmosphere to answer questions concerning the possible recovery of the ozone layer, air quality (i.e., pollution), and the changing climate. The OMI contributes to these mission objectives in all those fields.¹ The OMI is an ultraviolet–visible spectrometer with a wide instantaneous field of view (IFOV) perpendicular to the flight direction.² One can use the OMI measurements to study a number of

atmospheric trace gases, as well as aerosols and clouds. For ozone, NO₂, and SO₂ and various minor trace gases the total columns are retrieved for small ground pixels (at nadir, 13 km × 24 km). In addition, ozone profile information for the same ground scenes (at 13 km × 48 km resolution) is retrieved. The OMI is a successor to instruments such as the Global Ozone Monitoring Instrument³ (GOME), the Total Ozone Mapping Spectrometer⁴ (TOMS), the Solar Backscatter Ultraviolet Instrument⁴ (SBUV) and the Scanning Imaging Absorption spectrometer for Atmospheric Cartography (SCIAMACHY).⁵

The OMI can measure the Earth's radiance and the Sun's irradiance. Most retrieval algorithms use the sunlight that is scattered from the Earth and its atmosphere as the main input for their retrievals. For these algorithms to work properly, it is important that the instrument be calibrated accurately. For differential optical absorption spectroscopy (DOAs)-type retrieval algorithms^{6,7} that are used, e.g. for obtaining ozone and NO₂ total columns,^{8,9,10} the quality of the retrievals depends strongly on the accuracy of the wavelength calibration. The in-orbit calibration of the wavelength scale of OMI Earth spectra is the subject of this paper. The basic method used is similar to that used for previous satellite instruments and relies on fitting the solar Fraunhofer lines to a well-known solar reference spectrum.^{11,12} We show

All the authors are with KNMI/Royal Netherlands Meteorological Institute, P.O. Box 201, 3730 AE De Bilt, The Netherlands. R. Voors (voors@knmi.nl) is also with TUE/Eindhoven University of Technology, P.O. Box 513, 5600 MB Eindhoven, The Netherlands. R. Dirksen is also with SRON/Space Research Organization Netherlands, Sorbonnelaan 2, 3584 CA Utrecht, The Netherlands.

Received 25 October 2005; revised 15 December 2005; accepted 16 December 2005; posted 22 December 2005 (Doc. ID 65597).

0003-6935/06/153652-07\$15.00/0

© 2006 Optical Society of America

that the wavelength scale varies rapidly between measurements. These changes correlate strongly with the changes in the radiance signal that are often observed in the presence of clouds and snow and ice boundaries. We give an explanation for this unexpected and unprecedented behavior and describe the algorithm that corrects for it in the processing software that transfers the measured data into calibrated physical quantities.¹³

An outline of this paper is as follows: First, a description of the relevant instrumental properties is given. Next, we describe the in-flight behavior of the wavelength scale of the OMI Earth spectra and explain what causes the observed behavior. It is found that the observed effects are not restricted to the OMI alone but that they apply to other similar hyperspectral Earth observation spectrometers as well. Subsequently we describe how the processing software corrects for rapid changes in the wavelength scale and how well the correction algorithm performs. The paper ends with concluding remarks.

2. Ozone Monitoring Instrument

In this section we give an overview of the OMI. The information given is sufficient for understanding the remainder of the paper. For a more detailed description of the instrument and on-ground and in-flight calibration, see Refs. 13 and 14. The OMI is a push-broom nadir-viewing ultraviolet–visible (UV–VIS) spectrometer on board the EOS-Aura satellite. The instantaneous across-track field of view of the OMI is 115°, which results in daily global coverage. Sunlight scattered from the Earth and its atmosphere that enters the instrument is reflected off two telescope mirrors that project an image onto the entrance slit of the spectrograph. This slit is 44 mm long and 0.3 mm wide. The spectrograph is divided into two spectral channels: a UV and a VIS channel, that cover the wavelength ranges 270–370 nm and 350–500 nm, respectively. To suppress stray light, the UV channel is divided into two subchannels, UV1 and UV2, at ~310 nm. These and other properties of the OMI are listed in Table 1. Note that the spectral resolution and sampling are different for the different channels. The IFOV in the flight direction is ~1.0°, which corresponds to ~10 km on the ground.

The UV and VIS channels have separate CCD detectors of 780 pixels by 576 pixels in the spectral and across-track directions, respectively. So the spatial across-track information is expressed by the row number, and the spectral information by the column number. In nominal operational mode, the information in the across-track direction is binned by a factor of 8, resulting in 60 binned ground pixels in the UV2 and VIS channels and 30 in the UV1. In the flight direction, images are co-added to restrict the data rate. Typically two to five individual exposures (depending on the expected radiance levels) are co-added, resulting in co-addition factors of 2 to 5. For one column (wavelength) per CCD detector the individual readouts are retained. These are the so-called

Table 1. Properties of the OMI Instrument

Property	Value/Range
Spectral range	UV1/264–311 nm UV2/307–383 nm VIS/349–504 nm
Spectral sampling	UV1/0.33 nm/pixel UV2/0.14 nm/pixel VIS/0.21 nm/pixel
Spectral resolution (FWHM)	UV1/1.9 pixel = 0.63 nm UV2/3.0 pixel = 0.42 nm VIS/3.0 pixel = 0.63 nm
Telescope swath IFOV	115° (2600 km on the ground)
Telescope flight IFOV	1.0° (12 km on the ground)
Ground pixel size at nadir, global mode (electronic binning factor 8)	UV1/13 km × 48 km UV2/13 km × 24 km VIS/13 km × 24 km
Silicon CCD detectors	780 × 576 (spectral × spatial) pixels
Operational CCD temperature	UV/265.07 K VIS/264.99 K
In-orbit CCD temperature excursion	UV and VIS/ ±10 mK (stabilized)
Operational optical bench temperature	264 K
In-orbit optical bench temperature excursion	±300 mK
Orbit	Polar, Sun-synchronous: average altitude, 705 km (438 mi); orbit period, 98 min and 53 s; ascending node local time, 1:42 PM

small-pixel column radiances. These small-pixel column radiances are therefore available at a two-to-five-times higher frequency than the complete images, and for that reason they allow structures on the ground or in the atmosphere to be seen with a higher spatial sampling. The small-pixel columns were originally included in the design to permit the study of the effects of clouds. As is explained below, they will play a crucial role in in-flight wavelength assignment. The small-pixel column is column 267 in the UV2 channel (~340 nm) and column 219 in the VIS channel (~390 nm). Further details on the OMI and the OMI mission can be found elsewhere.^{1,2,13–15}

3. Wavelength Calibration of OMI Spectra

On-ground wavelength calibration of the OMI was performed with the well-known line lamp spectrum of a Pt–Cr–Ne hollow-cathode line lamp. The main drawback of this method is that the accuracy of the wavelength calibration is of the order of 1/10th of a pixel, because line blends and lack of available lines prevent higher accuracy. From scientific sensitivity studies it was determined that the required in-orbit knowledge of the wavelength scale is of the order of 1/100th of a pixel, which is ten times better than can be achieved with a line lamp spectrum. However, this accuracy can be reached by use of the solar Fraunhofer absorption lines in the Earth spectra. This method was also employed in previous satellite mis-

sions¹¹ and is similar to fitting a line lamp spectrum. The basis of the method is a high-resolution solar reference spectrum.¹² The wavelength scale of this spectrum is accurate to 0.002 nm below 300 nm and to 0.001 nm above 305 nm. This reference spectrum is convolved with the instrument transfer function (spectral slit function) to produce a simulated OMI solar measurement. The wavelength scale of this spectrum, effectively at the instrument's resolution, has the same accuracy as that of the original high-resolution spectrum, provided that the slit function is well known. For the OMI the spectral slit as a function of viewing angle and wavelength has been accurately calibrated on the ground by use of a purpose-built optical stimulus that utilizes an echelle grating.¹⁶ Thus the accuracy of the wavelength scale of the convolved spectrum is comparable to that of the original solar reference spectrum.

The original wavelength scale of a solar measurement is adjusted until it matches that of the convolved solar reference spectrum at OMI resolution. For sunlight scattered from the Earth and its atmosphere the same method is employed in principle, but, in addition to the Fraunhofer lines, these so-called Earth-reflected spectra also contain spectral structure originating from absorption and scattering that takes place in the Earth's atmosphere. The most important spectral structures are produced by ozone and by inelastic scattering, also known as the Ring effect.¹⁷ In calibrating the wavelength of an Earth-reflected spectrum, we fitted an optimal linear combination of these contributions, using a nonlinear solver based on a Levenberg-Marquardt algorithm.

The wavelength scale is known to vary with the temperature of the optical bench of the OMI. The temperature dependence was studied preflight and found to be small, typically a 0.01 pixel shift per kelvin. A temperature change over an orbit of at most a few tenths of a kelvin resulted in a change of a few thousandths of a pixel. Before launch, the wavelength scale was expected to vary mainly as a result of these temperature changes, so the wavelength scale was anticipated to be highly stable in flight.

With this in mind, as well as the considerable computational cost of performing wavelength calibration calculations for each individual spectrum and viewing angle, we decided to calculate the wavelength scale for each spectrum based on the wavelength scale given at a reference temperature (based on the wavelength calibration of a large number of solar spectra obtained at the reference temperature of 264 K) and the correction based on the temperature of the optical bench. Thus the wavelengths are assigned (predicted) rather than calibrated.¹³

In the calibrated product the wavelength scale is described by a polynomial rather than given for each sampled point. So, for each channel (UV1, UV2, VIS) and for each row in the measurement, the wavelength for column x is given by

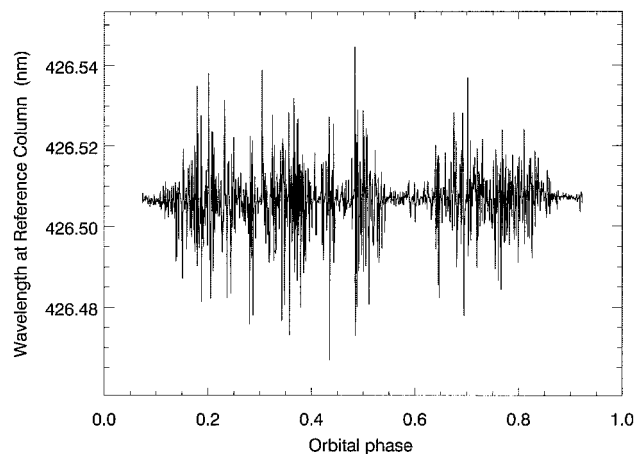


Fig. 1. Change in the wavelength of the reference column of the VIS channel during OMI orbit 3499 (12 March 2005) for the nadir-viewing pixel. Peak-to-peak variations are as much as 0.07 nm, or one third of a pixel. Only observations with a solar zenith angle of less than 85° are shown.

$$\lambda = \sum_{i=0}^n c_i (x - x_0)^i, \quad (1)$$

where x is the column number, x_0 is a reference column, c_i are the polynomial coefficients for the i th order, and n is the order of the polynomial, which is four for all channels.

4. Description of the Problem

When the first spectra came in, it soon became clear that the wavelength scale does not vary smoothly over an orbit, as expected from the observed temperature changes. Moreover, the amplitude of the wavelength variations is much larger than expected: The wavelength calibration shows differences of up to half a pixel, as shown in Fig. 1. We checked whether these variations were due to errors in the wavelength calibration, but several independent wavelength calibration methods yielded the same result. The observed variations do not correlate with changes in the temperature of the OMI optical bench, and the wavelength shifts induced by the temperature change are ~ 2 orders of magnitude smaller than the observed wavelength shifts.

As indicated above, the data processing system is not capable of performing wavelength calibration for each individual spectrum in terms of computational capacity but depends on the best available prediction or assignment. If the observed variations are not accounted for, the error in the predicted wavelength scale of the calibrated radiance product would be of the order of a few tenths of a pixel, which is in strong disagreement with the requirement of 1/100th of a pixel. In turn, such an error would lead to unacceptably large errors in higher-level DOAs products such as total column ozone, NO₂, and SO₂.¹⁸

Further investigation revealed that the rapid changes in the wavelength scale coincide with rapid changes in the radiances. Such changes often occur

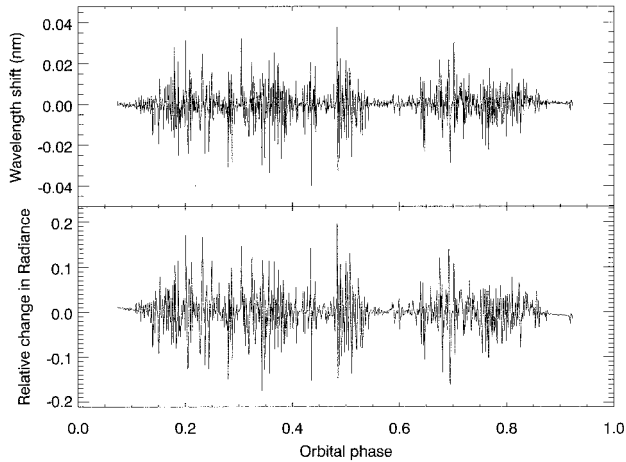


Fig. 2. Top, wavelength shift of the reference column of the central row in the VIS channel of orbit 3499 (12 March 2005). Bottom, relative change in the radiance. The correlation coefficient is 0.88, which suggests that the observed variations in the wavelength scale are causally related to the change in the radiance level.

near clouds and near snow and ice boundaries. Figure 2, top, shows for one orbit (3499, on 12 March 2005) of Earth measurements the absolute change in the wavelength for one column (i.e. one wavelength); at the bottom the relative change of the radiance signal is shown. The relative change is calculated as the radiance of the previous measurement minus the radiance of the next measurement divided by the sum of the two:

$$\Delta\text{Rad} = \frac{\text{Rad}(i+1) - \text{Rad}(i-1)}{\text{Rad}(i+1) + \text{Rad}(i-1)}. \quad (2)$$

The correlation coefficient between the wavelength change and the change in the radiance signal is 0.88 for this case, which suggests that the two are causally related.

5. Optical Explanation

One can understand the findings described above by taking a closer look at the optics of the OMI. Sunlight that is reflected from the Earth and its atmosphere enters the instrument via the telescope, which focuses the light on the spectrograph's entrance slit. The way in which this spectrograph images a monochromatic narrow beam onto the CCD detectors is described by the so-called spectral slit function. Both the shape and the width of these spectral slit functions were accurately determined on the ground for all wavelengths and all viewing angles.¹⁶ The exact shape of the slit function has an immediate effect on the wavelength calibration. The spectral slit function was found to exhibit some degree of asymmetry. If instead of the real asymmetric slit function a symmetric slit function of the same width is assumed, the wavelength scale of the solar reference spectrum (i.e., the high-resolution solar spectrum convolved with the OMI slit function) can change by as much as

0.03 nm. And, because the wavelength scale of the solar reference spectrum determines the wavelength scale of the OMI measurement, this change has a nonnegligible effect.

When the observed ground scene does not fill the spectrometer's entrance slit homogeneously in the flight direction, for example in the case of clouds, the shape and the position of the maximum of the spectral slit function change. The OMI's instantaneous field of view in the flight direction is 1.0°, corresponding to ~10 km on the ground, which is a typical size for clouds. The change in shape and position of the spectral slit function subsequently leads to an observed shift in the wavelength mapping of the solar Fraunhofer lines on the CCD detectors. These are the wavelength shifts that we observe in the Earth measurement data as clouds move in and out of the field of view in the flight direction.

It must be noted that the effect described above is not typical for the OMI alone but can also play an important role in other hyperspectral Earth observation spectrometers with comparable resolution and field-of-view size. However, scanning spectrometers such as the GOME and the SCIAMACHY will suffer less from this effect because they scan a much larger ground scene. This has an averaging effect on the observed shifts.

6. Correcting for Rapidly Changing Radiances

During a coadded (typical coadding factor, 2–5; see above) OMI measurement, the radiances of the observed scene may vary quickly, mostly as a result of scattering by clouds. Fortunately, for nearly all of recorded spectra, we have knowledge of the radiance history during one complete coaddition period, by means of the small-pixel column radiances. These can be used to predict the change in the wavelength scale. As was shown above, there is a strong correlation between the observed change in wavelength scale and the relative change in radiance between two subsequent measurements. By use of the small-pixel radiances we can actually see what happened during the measurement itself, because the small-pixel column radiances are available at a higher time resolution than the complete images.

When we make the same comparisons as above but now replace the relative change between two measurements by the relative change during the measurement, we see that the correlation is even better (see Fig. 3). This result is fully representative for all orbits and viewing angles. The relative change is calculated as the difference between the last and the first small-pixel radiance for a coaddition period divided by the sum of those two:

$$\Delta\text{Rad}_{\text{smp}} = \frac{\text{Rad}_{\text{smp}}(\text{last}) - \text{Rad}_{\text{smp}}(\text{first})}{\text{Rad}_{\text{smp}}(\text{last}) + \text{Rad}_{\text{smp}}(\text{first})}, \quad (3)$$

where $\Delta\text{Rad}_{\text{smp}}$ indicates the small-pixel column radiance.

The next step is to use these dependencies to come

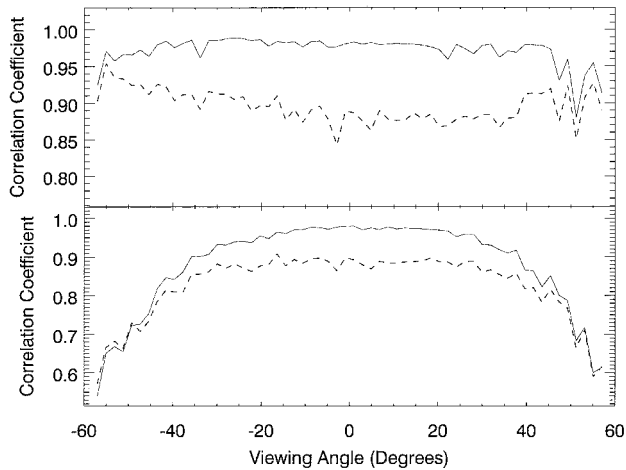


Fig. 3. Correlation coefficient between the observed wavelength shift and the rate of change in the radiance for orbit 3499 (12 March 2005). Top, VIS channel; bottom, UV2 channel. dashed curves, result when the change in the radiance is calculated from the difference between two neighboring images. Solid curves, rate of change in the radiance calculated based on the small-pixel radiances, which results in an even better correlation.

to a better in-flight determination of the wavelength scale. For each wavelength (column) and viewing angle (row) we calculate the conversion factor needed to convert the observed rate of change in radiance to an equivalent shift in wavelength:

$$\Delta\lambda(\text{row}, \text{col}) = F(\text{row}, \text{col})\Delta\text{rad}(\text{row}, \text{col}), \quad (4)$$

where $\Delta\lambda$ is the shift in wavelength (in nanometers), F is the conversion factor, and Δrad is the observed rate of change in the small-pixel column radiance. These conversion factors are different for the different channels.

With these conversion factors for the UV2 and VIS channels we can correct the wavelength scale by using the observed rate of change of the small-pixel column radiance. In Fig. 4 we show how well this correction works. At the top left of Fig. 4 we show the relative change in the first wavelength polynomial coefficient for the VIS channel for orbit 3499. The top right shows the relative change in radiance multiplied by the precalculated conversion factor. At bottom left we show the difference between the two changes. At the bottom right we show the observed shift (delta calibration) versus the precalculated shift (delta assignment).

For the UV1 channel there is no clear correlation between the observed wavelength shift and the relative change in the radiance (correlation coefficient, <0.2). The reason for this is that, at these short wavelengths (<310 nm), light is reflected high in the atmosphere, well above the Earth's surface and the majority of the clouds. This means that relative changes in the radiance are much smaller at these wavelengths than, e.g., in the VIS channel. As a result, the variability of the wavelength scale during an orbit is much smaller. In fact, it is smaller than the

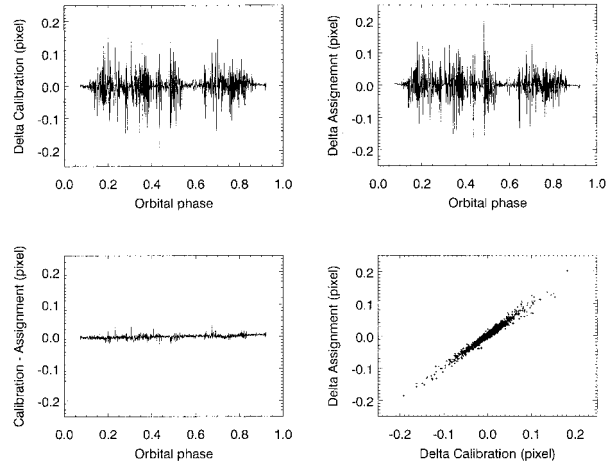


Fig. 4. Top left, relative change in the first wavelength polynomial coefficient for a nadir pixel in the VIS channel for orbit 3499 (12 March 2005), expressed in pixels. Top right, relative change in radiance multiplied by a precalculated factor. Bottom left, difference between the two. Bottom right, observed shift (delta calibration) versus the precalculated shift (delta assignment).

requirement for accuracy in that channel, which is 1/50th of a pixel. Thus there is no need to correct the wavelength scale in the UV1 channel. So the wavelength scale of the UV1 channel is left unchanged after the initial wavelength assignment step.

It should be noted that the root-mean-square (RMS) difference between the calibration (Fig. 4, top left) and the assignment (Fig. 4, top right) is only an indication of how well the correction works; it is not a direct measure. The reason for this is that the wavelength calibration is not infinitely accurate. In the VIS channel the wavelength calibration is expected to be highly accurate, but in the UV channel, especially at high solar zenith angles, the effect of ozone on the signal and therefore on the wavelength calibration becomes noticeable. This can also be seen from Fig. 3: At large viewing angles in the UV2 channel the correlation coefficient decreases. This may be the result of the increased influence of ozone on these Earth-reflectance spectra.

The results shown in Fig. 4 are representative for all orbits and all viewing directions in the UV2 and VIS channels. In Fig. 5 we show the RMS difference as introduced above, for the VIS channel for orbit 3499 (12 March 2005), for all viewing angles. The results are consistent for both channels and all orbits. In most cases the RMS residual is below 1/100th of a pixel.

7. Operational Algorithm

To be able to correct for the observed wavelength shifts, it is important that the derived conversion factors be stable in time. For example, the conversion factors derived based on the first half of an orbit should be the same as those based on the second half. In addition, they should not change over longer periods of time, i.e., between orbits. These requirements turn out to be fulfilled. This means that we can pre-

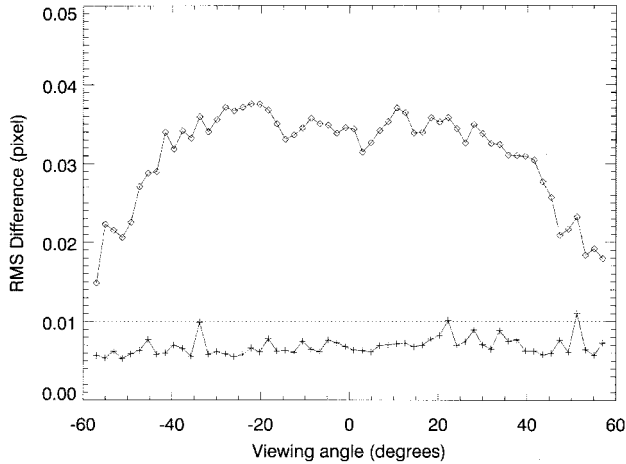


Fig. 5. RMS difference in the VIS channel for orbit 3499 (12 March 2005) of the wavelength shift calculated by the spectral calibration and by the rate of change in the small-pixel radiance. The RMS before correction for the inhomogeneous illumination of the entrance slit is shown by diamonds; the pluses give the result after correction. Dotted line, requirement of knowledge of the wavelength scale. It can be clearly seen that the correction brings the reported wavelength scale within the required accuracy.

calculate the conversion factors, based on a large number of orbits, to increase statistics and decrease noise, and apply those numbers to all observations. The orbit-to-orbit variability is of the order of 5% for the correction factors for the first wavelength polynomial. This variability is mainly statistical and is largely reduced by averaging the correction factors of a large number of orbits spread over a long period of time. The error in the derived correction of the wavelength scale that is due to the inhomogeneous slit illumination is of the order of 1%–2%. So, for an initial shift of 0.1 pixel, the error made amounts to $\sim 1/500$ th to $\sim 1/1000$ th of a pixel.

So far, we have considered only the change in the first polynomial coefficient of the wavelength parameterization. This is clearly the most important effect. However, we have also found that the amplitude of wavelength shift is dependent on the wavelength itself. That is, the effect that, e.g., a passing cloud has on the spectral slit function is wavelength dependent. This is to be expected, because the slit function is wavelength dependent as well. Therefore, not only the first parameter in the wavelength parameterization, but higher-order terms as well, need to be modified. This is also expressed by the fact that the relative change in the signal is strongly correlated not only with the first polynomial coefficient but with the second as well.

In the data processor, the polynomial coefficients that describe the wavelength [see Eq. (1)] are modified:

$$c_i = c_i^{\text{initial}} + b_i \Delta \text{Rad}_{\text{smp}}, \quad (5)$$

where c_i^{initial} are the wavelength coefficients after the small temperature correction has been applied and b_i

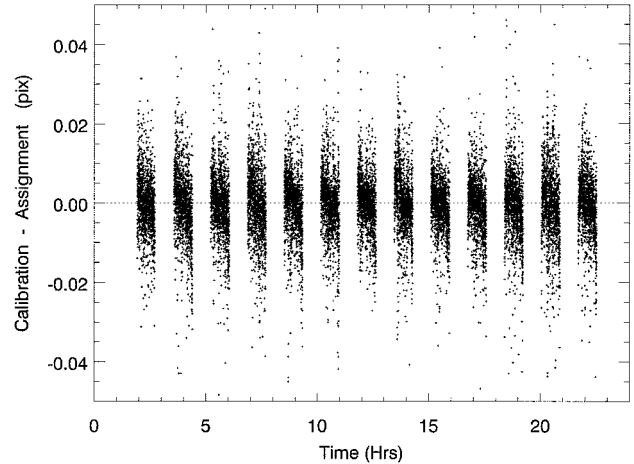


Fig. 6. Difference between the wavelength calibration and assignment in the calibrated level 1 product for one day of data (4 September 2005) for the VIS channel. The RMS of the difference is 0.008 pixels. The UV2 channel gives similar results.

are the precalculated conversion coefficients. After that, the wavelengths are calculated from Eq. (1).

This method was integrated into the data processing software in February 2005 and was found to work as expected. As an example we show the results of 4 September 2005 (Fig. 6). For this day we have plotted the difference between the calibrated wavelengths and the wavelengths as assigned in the calibrated level 1 product, for the nadir row. We found that the RMS of the difference is 0.007 and 0.008 pixel for the UV2 and VIS channels, respectively. It should be noted that not all this difference can be ascribed to the error in the correction method. The wavelength calibration itself also contains some uncertainty.

8. Conclusions

In this paper we have described in-flight wavelength calibration for the Ozone Monitoring Instrument. Large and rapid variations in the wavelength scale up to a few hundredths of a nanometer were found above 300 nm. The observed effects are explained by inhomogeneous filling, mainly by clouds, of the spectrometer's entrance slit in the flight direction, which changes the shape and position of the spectral slit functions, which in turn yields the observed wavelength shifts. A method based on the signal variations of the small-pixel column radiances was developed to correct for the observed wavelength shifts in the UV2 and VIS channels. We have shown that this correction works well and that the requirement on the knowledge of the wavelength scale (0.01 pixel) is met for nearly all observations. We suspect that the wavelength shift mechanism plays an important role in other hyperspectral Earth observation instruments with similar instrument characteristics (wavelength sampling, resolution, and size of the field of view in the flight direction).

This research was funded by the Netherlands Agency for Aerospace Programmes (NIVR) within

the framework of the Ozone Monitoring Instrument (OMI) project. We thank G. H. J. van den Oord for fruitful discussions and his contributions to this paper.

References

1. P. F. Levelt, E. Hilsenrath, G. W. Leppelmeier, G. H. J. van den Oord, P. K. Bhartia, J. Tamminen, J. F. de Haan, and J. P. Veefkind, "Science objectives of the Ozone Monitoring Instrument," *IEEE Trans. Geosci. Remote Sens.* (to be published).
2. P. F. Levelt, G. H. J. van den Oord, M. R. Dobber, J. Claas, H. Visser, and J. de Vries, "The Ozone Monitoring Instrument," *IEEE Trans. Geosci. Remote Sens.* (to be published).
3. J. P. Burrows, M. Weber, M. Buchwitz, V. Rozanov, A. Ladstätter-Weissenmayer, A. Richter, R. De Beek, R. Hoogen, K. Bramstedt, K. W. Eichmann, M. Eisinger, and D. Perner, "The Global Ozone Monitoring Experiment (GOME): mission concept and first scientific results," *J. Atmos. Sci.* **56**, 151–175 (1999).
4. D. F. Heath and H. Park, "The Solar Backscatter Ultraviolet (SBUV) and Total Ozone Mapping Spectrometer (TOMS) experiment," in *The Nimbus-7 Users Guide*, C. R. Madrid, ed. (NASA Goddard Space Flight Center, (1978), pp. 175–211).
5. J. P. Burrows, E. Hoelzle, A. P. H. Goede, H. Visser, and W. Fricke, "SCIAMACHY—Scanning imaging absorption spectrometer for atmospheric cartography," *Acta Astron.* **35**, 445–451 (1995).
6. R. Spurr, "GOME Level 1 to 2 algorithms description," Tech. Note ER-TN-DLR-GO-0025 (DLR, Oberpfaffenhofen, Germany, 1994).
7. J. P. Veefkind, J. F. de Haan, E. J. Brinksma, M. Kroon, and P. F. Levelt, "Total ozone from the Ozone Monitoring Instrument (OMI) using the DOAS technique," *IEEE Trans. Geosci. Remote Sens.* (to be published).
8. P. K. Bhartia, R. D. McPeters, L. E. Flynn, and C. G. Welle-meyer, "Highlights of the Version 8 SBUV and TOMS datasets released at this symposium," in *Proceedings of the XX Quadrennial Ozone Symposium*, C. S. Zerefos, ed. (International Ozone Commission, 2004), p. 294.
9. K. F. Boersma, H. J. Eskes, and E. J. Brinksma, "Error analyses for tropospheric NO₂ retrieval from space," *J. Geophys. Res.* **109**, D04311 (2004).
10. M. Dobber, R. Dirksen, R. Voors, G. H. Mount, and P. Levelt, "Ground-based zenith sky abundances and *in situ* gas cross sections for ozone and nitrogen dioxide with the Earth Observing System Aura Ozone Monitoring Instrument," *Appl. Opt.* **44**, 2846–2856 (2005).
11. J. H. G. M. van Geffen, "Wavelength calibration of spectra measured by the Global Ozone Monitoring Instrument: variation along orbits and in time," *Appl. Opt.* **43**, 695–706 (2004).
12. K. Chance and R. J. D. Spurr, "Ring effect studies: Rayleigh scattering, including molecular parameters for rotational Raman scattering, and the Fraunhofer spectrum," *Appl. Opt.* **36**, 5224–5230 (1997).
13. G. H. J. van den Oord, J. P. Veefkind, P. F. Levelt, and M. R. Dobber, "Level 0 to 1B processing and operational aspects," *IEEE Trans. Geosci. Remote Sens.* (to be published).
14. M. R. Dobber, R. J. Dirksen, P. F. Levelt, G. H. J. van den Oord, R. Voors, Q. Kleipool, G. Jaross, M. Kowalewski, E. Hilsenrath, G. Leppelmeier, J. de Vries, W. Dierssen, and N. Rozemeijer "Ozone monitoring instrument calibration," *IEEE Trans. Geosci. Remote Sens.* (to be published).
15. J. de Vries, R. H. M. Voors, R. Dirksen, and M. Dobber, "In-orbit performance of the Ozone Monitoring Instrument," in *Sensors, Systems, and Next-Generation Satellites IX*, R. Meynart, S. P. Neeck, and H. Shimoda, eds., *Proc. SPIE* **5978**, 234–245 (2005).
16. R. Dirksen, M. Dobber, R. Voors, and P. Levelt, "Ozone monitoring instrument pre-launch characterization of the instrument transfer function in the spectral domain," *Appl. Opt.* (to be published).
17. J. F. Grainger and J. Ring, "Anomalous Fraunhofer line profiles," *Nature* **193**, 762–764 (1962).
18. OMI Algorithm theoretical basis documents, www.knmi.nl/omi/research/documents (August 2005).